Theoretical considerations of chemical reactions in micro-reactors operating under electroosmotic and electrophoretic control

The Analyst
Tutorial Review

Paul D. I. Fletcher,* Stephen J. Haswell and Vesselin N. Paunov

Department of Chemistry, University of Hull, Hull, UK HU6 7RX.
E-mail: p.d.fletcher@chem.hull.ac.uk

Received 6th May 1999, Accepted 7th July 1999

Summary of contents

1 Introduction

Since the introduction of the concepts of micro flow injection analysis (μFIA) and micro total analytical systems (μTAS) nearly a decade ago;[1–3] few researchers in the field of analytical science can fail to have been impressed by their impact, particularly in the area of DNA diagnostics.[4–10] From the literature one is able to trace the pioneering developments of fabrication[11–19] through detection[20–26] and separation[23,24,27–32] to sample preparation,[5,33–35] culminating, for example, in a recent paper by Waters *et al.*[34] which describes a fully integrated μTAS device for DNA characterisation. Whilst the majority of μFIA and μTAS studies have been focused on their application as capillary electrophoresis (CE) separation systems,[23,24,27–32] the opportunity exists to extend such micro-reactor technology into the concept of 'Lab-on-a-Chip'.[36–39] In this approach, the possibility exists of using a microfabricated system for the full characterisation of a wide range of chemical processes. Realisation of this goal requires a better understanding of the fluidics of chemically reacting systems in micro-reactors.

Whilst hydrodynamically pumped systems have been described in the literature,[40–43] it has been the application of electrokinetic based fluidic pumping that has dominated previous studies.[44–46] This clear trend can be attributed to

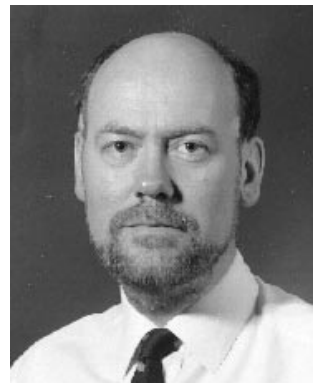

Stephen Haswell is Professor of Analytical Science at the University of Hull. His current research activities are in the areas of micro-reactor and μFIA development, microwave enhanced reaction chemistry, trace elemental speciation and process analysis. He is author of over 100 research papers, a number of books and patents and is widely known nationally and internationally for his enthusiastic lectures. For a number of years one of the underlying principles of Professor Haswell's research has been to break down the sectorial walls which exist in science, in particular, the integration of analytical science with main line chemistry, physics, engineering and biology. Many of these ideals are encompassed in the development of micro-chemical processes and devices, part of which is reflected in this current review.
E-mail: S.J.Haswell@chem.hull.ac.uk

Paul Fletcher is Professor of Physical Chemistry at the University of Hull. He leads the Surfactant Science Group within the Department of Chemistry and his research interests include micro-reactors and the surface and colloid chemistry of surfactant systems such as micelles, monolayers, microemulsions, emulsions and foams and reactions in complex media. He has published over 100 papers in these areas.
E-mail: P.D.Fletcher@chem.hull.ac.uk

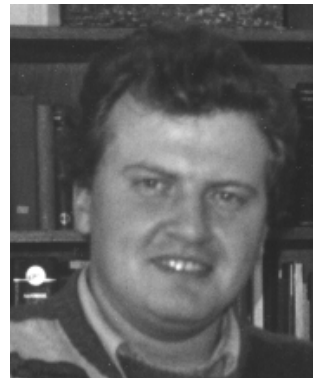

Vesselin N. Paunov is a Postdoctoral Fellow at the Department of Chemical Engineering of the University of Delaware. His research interests include surface forces and stability of foams and emulsions, wetting and spreading, capillary forces between colloidal particles, electrokinetic phenomena, phase behaviour and microstrucutre of complex fluids, and computer modelling of physicochemical processes and micro-reactors. He has published over 25 papers in these areas.
E-mail: paounov@che.udel. edu

factors such as the experimental simplicity in achieving electroosmotic flow, *i.e.*, no moving parts, and minimal back-pressure effects, with the added dimension of superimposed electrophoretic separations. It follows, therefore, that a good basic understanding of the nature and capability of electro-kinetic based devices is fundamental to the design and development of future applications. A number of theoretical and experimental studies of hydrodynamic and electrokinetic flow within μFIA and μTAS, including channel switching and velocity profile control, have been reported.[47–52]

In this tutorial review, we describe the basic theoretical considerations governing liquid phase chemical reactions in micro-reactor manifolds using electrokinetic based fluidics. The calculations described demonstrate how the voltages applied may be used to control both the spatial (*i.e.*, lengthways along the channel long axis) and temporal evolution of chemical components and reaction products. The combination of spatial and temporal control of reactions, realisable in such micro-reactor manifolds (but not, for example, in microtitre wells), offers many potential advantages such as identifying the optimum detector position and the best point at which to perform reagent additions in catalytic systems. The purpose of this work is to review the quantitative theoretical basis for this type of control and to provide illustrative calculations to guide the design and development of novel micro-reactor systems.

The paper is organised as follows. First, the basic principles of electroosmotic flow (EOF) and electrophoresis are described. We then consider a specific micro-reactor manifold configuration and show how the operating voltages can be adjusted to control the loading, injection and flow phases necessary to investigate analytical type chemical reactions. The next section details the equations describing the spatial and temporal evolution of chemical reactions under EOF and electrophoretic control. Numerical results are then presented which illustrate the main features of the behaviour of chemical reactions under voltage control. Finally, the conclusions and the outlook for the future are discussed.

2 Electroosmotic flow and electrophoresis in micro-reactor manifolds

Fabrication of μFIA or μTAS micro-reactor manifolds involves creating a network of micron sized channels in a solid substrate surface using either wet etch, laser ablation, embossing, micromachining or microlithography techniques.[11–19,53–56] Suitable substrates include materials such as glass, oxidised silicon and various plastics which support EOF. In most fabrication procedures a top cover is then bonded to the substrate using anodic or fusion bonding.[53,56] Holes drilled through the top cover allow connection to the channels and also form the reagent reservoirs. Voltages to drive EOF are applied through electrodes placed within the reservoirs. With this form of fabrication the channels approximate to a rectangular cross-section with depths in the range 10–200 μm, widths of 50–200 μm and lengths in the centimetre range, as shown in Fig. 1. The reagent reservoirs are typically 1 mm in diameter and 1 cm in depth. A plan view of an entire micro-reactor manifold (as used in recent analytical studies[57,58]) is shown in Fig. 1. For the purposes of this paper, we shall consider parameters appropriate to glass micro-reactor manifolds containing aqueous solutions of reactant species X and Y that react to form a product Z which can be detected colorimetrically.

For pure electroosmotic flow within a channel, the velocity profile across the channel is uniform except for the region very close to the channel wall.[50,59,60] The thickness over which the velocity is non-uniform is of the order of the Debye length and is in the nanometer range. The linear liquid velocity far from the walls due to electroosmosis v_{os} is[60]

$$v_{os} = -\frac{E\varepsilon\varepsilon_0\zeta}{\eta} \quad (1)$$

where E is the electric field (equal to the voltage divided by the distance between the electrodes for channels of uniform resistance per unit length), ε is the relative permittivity of the liquid, ε_0 is the permittivity of free space, ζ is the zeta potential of the channel/liquid interface and η is the liquid viscosity. The negative sign indicates that when ζ is negative, the diffuse charge in the liquid is positive and so the liquid flow is towards the negative electrode. The volumetric flow rate due to electroosmotic flow is $V_{os} = A_{channel}v_{os}$, where $A_{channel}$ is the cross-sectional area of the channel. The electric current I transported by the liquid is proportional to v_{os} according to

$$I = \frac{A_{channel}v_{os}\eta\lambda_0}{\varepsilon\varepsilon_0\zeta} \quad (2)$$

where λ_0 is the electrical conductivity of the liquid. Eqn. (2) neglects the possibility of surface conduction, which can be a complicating factor under some conditions.[60]

It can be seen that the EOF is primarily controlled by the zeta potential at the channel wall/solution interface. For aqueous solutions in glass channels the zeta potential varies from zero at pH ≈ 2 to about −100 mV at pH 7.[61–64]

At fixed pH, the magnitude of ζ decreases with increasing concentration of most common electrolytes.[61–64] It should be noted that the presence of species such as cationic surfactants, which adsorb strongly at the glass/water interface, can strongly influence ζ and hence the EOF.[65] The zeta potential is also sensitive to the nature of the glass and its treatment.[61] For aqueous solutions around pH 7 (for which ζ is around −100 mV) with E of the order of 100 V cm^{-1}, v_{os} is of the order of mm s^{-1}.

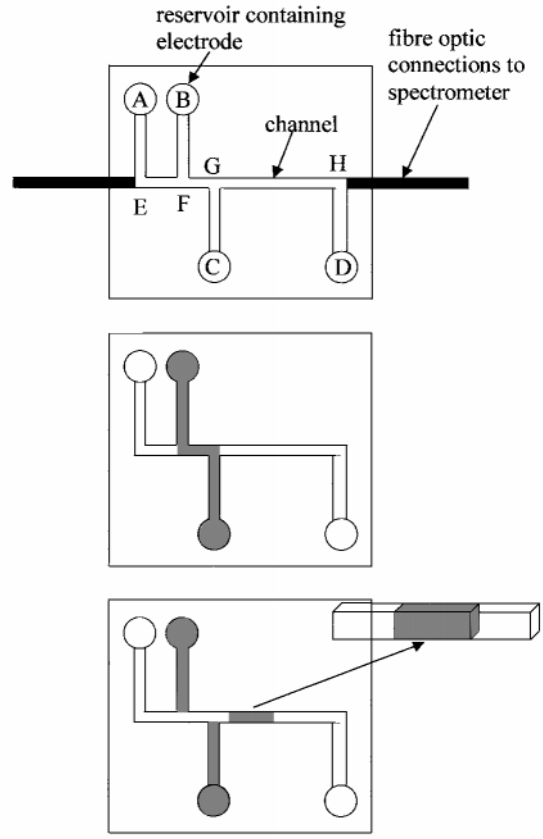

Fig. 1 Plan view of the basic micro-reactor configuration (not to scale). The reservoir diameters are typically 1 mm, the channel widths are typically 100 μm and the side length of the microreactor is typically 2 cm. The middle diagram shows channel BC filled with Y. The bottom diagram shows the experimental configuration modelled here in which a stream of X containing a slug of Y (shown in 3D view in inset) is moving by EOF towards reservoir D.

Note that pure electroosmotic flow is only obtained in the absence of a pressure difference ΔP across the tube. If ΔP is not zero, one obtains a combination of electroosmotic and pressure driven flow. Since pressure driven flow (in a cylindrical channel) shows a parabolic velocity profile, a flat velocity profile across the channel is only obtained when ΔP is negligibly small. Experimentally, non-negligible pressure differences may be caused by a difference in liquid levels between the inlet and outlet reservoirs (Δh_{res}), by Laplace pressure differences resulting from the curved liquid menisci in the inlet and outlet reservoirs or by obstruction within the channel leading to a back-pressure.

The Laplace pressure change across the liquid menisci within the reservoirs is equal to $2\gamma/r$, where γ is the liquid/air surface tension and r is the radius of curvature of the liquid meniscus. As in capillary rise phenomena,[66] the radius of curvature of the liquid meniscus depends on both the radius of the reservoir containing the surface (r_r) and the contact angle θ made by the liquid with the reservoir wall according to $r = r_r/\cos\theta$. For pure water of tension 72 mN m^{-1} making a contact angle of 0° within a cylindrical reservoir of radius 1 mm, the Laplace pressure is approximately 140 Pa. The magnitude of this Laplace pressure, equivalent to the hydrostatic pressure exerted by a column of water of approximately 14 mm in height, can be significant in considerations of flow within micro-reactors.

Within a micro-reactor, a non-zero ΔP from Laplace effects arises only when the Laplace pressure *differences* across the inlet and outlet reservoirs are not equal. Since the liquid menisci within the inlet and outlet reservoir are normally similar, ΔP values from Laplace effects are generally expected to be considerably smaller than the value quoted above for a single meniscus. For a cylindrical reservoir containing an electrode, the meniscus shape is complex and the Laplace pressure will depend on the positioning of the electrode within the reservoir, the contact angles of the liquid with the electrode and the reservoir wall in addition to the tension. The value of ΔP arising from Laplace pressure differences can be minimised by matching reservoir diameters and electrode positioning for the inlet and outlet reservoirs as far as possible. The Laplace pressure can be reduced to zero if the reservoir diameter is made sufficiently large such that the liquid surface contains a flat region. This situation applies when the reservoir radius is much greater than the length scale over which the liquid meniscus is curved, *i.e.*, the capillary length equal to $\sqrt{\gamma/\Delta\rho g}$, where $\Delta\rho$ is the density difference between the liquid and air and g is acceleration due to gravity.

In order to ensure that 'pure' EOF is obtained within a channel, it is necessary to consider the limits of ΔP within which the pressure driven component of the total flow can be considered negligible relative to that from EOF. In the case that Laplace pressures and channel obstruction effects are absent, *i.e.*, ΔP arises only from hydrostatic pressure resulting from a difference in reservoir liquid height Δh_{res} ($\Delta P = \Delta h_{res}\Delta\rho g$), this can be estimated as follows. We consider the magnitude of Δh_{res} sufficient to produce a pressure driven volumetric flow rate V_{press} equal to V_{os}. We estimate V_{press} for laminar flow within a cylindrical channel of 'effective' radius r_{eff} such that $\pi r_{eff}^2 = A_{channel}$ and equate this with V_{os}:

$$V_{press} = \frac{\pi\Delta h_{res}\rho g r_{eff}^4}{8\eta l_{channel}} = V_{os} = \frac{V\varepsilon\varepsilon_0\zeta}{\eta l_{channel}} \quad (3)$$

where $l_{channel}$ is the channel length held between the reservoirs and V is the voltage applied between the reservoirs. Rearrangement of eqn. (3) shows that, for V_{press} to be less than 10% of V_{os}, then

$$\Delta h_{res} \leqslant \frac{V\varepsilon\varepsilon_0\zeta}{10\rho g r_{eff}^2} \quad (4)$$

Inspection of eqn. (4) shows that for many μTAS operating conditions described in the literature, Δh_{res} may have to be less than 1 mm of water pressure in order to suppress pressure driven flow. Depending on the conditions (*e.g.*, whether the feed reservoir height is greater or less than the destination reservoir), the pressure driven flow may either accelerate or retard the EOF. For either acceleration or retardation, pressure driven flow will perturb the flat velocity profile expected for 'pure' EOF. Disturbances of EOF by pressure effects have been demonstrated experimentally by Boer *et al.*[46] Lack of proper control of these small pressure differences is expected to lead to irreproducible and erratic experimental results.

In addition to EOF, charged species within the channels move under the influence of the electric field by electrophoresis. The electrophoretic velocity v_{ph} of a species is given by[67]

$$v_{ph} = \frac{zeED}{kT} \quad (5)$$

where z is the number of electronic charges on the species (positive for cations, negative for anions), e is the electronic charge (magnitude only), D is the diffusion coefficient, k is the Boltzmann constant and T is the absolute temperature. The total velocity of a particular species is simply the vector sum of that due to the electroosmosis and electrophoresis, *i.e.*, $v_{total} = v_{ph} + v_{os}$. For aqueous solutions in a glass channel (where ζ is negative), a positive value of v_{os} signifies movement towards the negative electrode. In this situation, the electrophoretic velocities of cations (z positive) are increased relative to v_{os} whereas the velocities of anions are decreased. For common small ions, the magnitudes of v_{ph} and v_{os}, both of which scale with E, are generally similar and in the mm s^{-1} range.

3 Micro-reactor manifold configuration

In this section we present explicit calculations for the simple micro-reactor manifold configuration shown as a plan view in Fig. 1. It consists of four reservoirs (A, B, C and D) each containing an electrode and connected by etched channels. The lengths of the different channel sections are specified here by reference to the letters marking the corner points as shown in Fig. 1. We shall consider a bimolecular, reversible reaction which, in analytical terms, could be the formation of a chromogenic complex:

$$X + Y \rightleftharpoons Z \quad (6)$$

The reaction has a forward, second-order rate constant k_f and reverse, first-order rate constant k_r. For the configuration shown, detection of the reaction progress is provided by optical absorbance measurements along the EH channel section situated between fibre optics connected to a spectrophotometer. Although the theoretical results presented here refer to the specific configuration of Fig. 1, the calculation approach may be easily modified to apply to a very wide range of manifold designs with more complex channel labyrinths and different detection systems.

The reactant species X and Y are introduced into the micro-reactor as follows. Initially, all reservoirs and channels are filled with solvent. The solution of reactant X is introduced into reservoir A and a suitable voltage is applied across the electrodes within the reservoirs A and D to fill the AD channel with X (the 'loading' phase). Reactant Y is introduced into reservoir B and a voltage across BC is used to fill the BC channel (the 'injection' phase) as shown in Fig. 1 (middle). For the experimental situation to be modelled, a voltage is reapplied across AD which mobilises the stream of X, now containing a slug of Y, in the EH channel (the 'flow' phase, Fig. 1, bottom). In fact, as will be discussed in detail in the next section, suitable voltages across *both* AD and BC must be applied simultane-

ously for the loading, flow and injection phases in order to achieve a 'clean' injection. The progress of the reaction of the slug of Y within the flowing stream of X is then monitored by the fibre optic spectroscopic detection systems and is considered in detail in the calculations presented later.

4 Voltage conditions for loading, flow and injection

As discussed by Seiler *et al.*,[49] dc circuit analysis (using Kirchhoff's rules) can be used to predict the variation with applied voltages of the electrical currents, and hence EOFs, in the different channel sections of a manifold. The manifold configuration of Fig. 1 can be represented as the equivalent dc circuit shown in Fig. 2. The circuit consists of two voltage sources V_{AD} and V_{BC} (supplied by the electrode pairs in reservoirs AD and BC, respectively) connected by the appropriate channel sections which form resistance elements R_{IJ}, where the subscripts signify the particular channel section. The overall circuit contains two loops which both contain R_{FG}. We assume here that all channel sections have a uniform cross-sectional area and zeta potential and all contain liquid of identical conductivity. Under these conditions, easily achievable with solutions containing low concentrations of reacting species in a relatively high concentration of inert electrolyte, the resistance of a channel section is proportional to its length. We note that the approach could be extended to the more complex case where the resistance per unit length of the channel is not constant in different parts of the manifold. Neglecting surface conductivity, the electrical currents (proportional to the EOF velocity as discussed earlier) in the arms of loops 1 and 2 are I_1 and I_2, respectively. The current in the FG channel section (common to both loops) is $I_1 + I_2$. Summing the product of current and resistances around each loop gives the following pair of equations:

$$\begin{aligned} V_{AD} &= (R_{AE} + R_{EF} + R_{GH} + R_{HD} + R_{FG})I_2 + R_{FG}I_1 \\ &= R_{loop\,2}I_2 + R_{FG}I_1 \\ V_{BC} &= (R_{CG} + R_{FB} + R_{FG})I_1 + R_{FG}I_2 \\ &= R_{loop1}I_1 + R_{FG}I_2 \end{aligned} \quad (7)$$

Solving the simultaneous equations and rearranging yields the following expressions for I_1 and I_2:

$$I_1 = \frac{V_{BC} - V_{AD}R_{FG}/R_{loop\,2}}{R_{loop\,1} - R_{FG}^2/R_{loop\,2}}$$

$$I_2 = \frac{V_{AD} - V_{BC}R_{FG}/R_{loop\,1}}{R_{loop\,2} - R_{FG}^2/R_{loop\,1}} \quad (8)$$

The current through the FG channel section is $I_1 + I_2$. Eqn. (8) allows the currents, and hence the EOF, in each channel section to be calculated for any voltages provided that the resistances of the different channel sections are known.

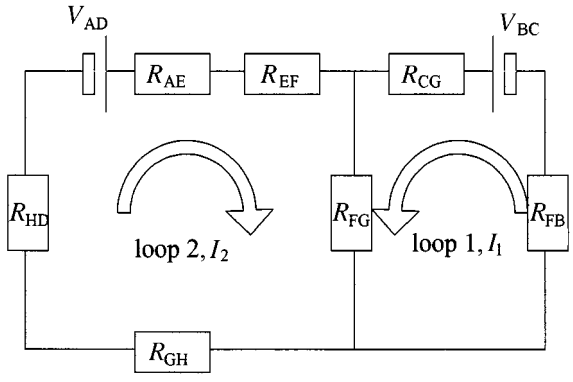

Fig. 2 The dc circuit equivalent to the micro-reactor configuration of Fig. 1. The rectangular boxes are the resistance elements arising from the channel sections marked by the subscripts.

For the loading and flow phases, we require EOF (*i.e.*, finite current I_2) between reservoirs A and D with zero EOF between reservoirs B and C (*i.e.*, current I_1 equal to zero) to avoid contamination of one reactant stream with the other. Similarly, for the injection phase, finite current I_1 and zero current I_2 are required. Inspection of eqn. (8) shows that, in order to obtain zero I_1, the voltages V_{AD} and V_{BC} must obey the relationship

$$V_{BC} = V_{AD}R_{FG}/R_{loop\,2} = V_{AD}\text{length}_{FG}/\text{length}_{loop\,2} \quad (9)$$

The second equality is valid in the case that the resistance per channel length is constant. Similarly, to obtain zero I_2, we require

$$V_{AD} = V_{BC}R_{FG}/R_{loop\,1} = V_{BC}\text{length}_{FG}/\text{length}_{loop\,1} \quad (10)$$

Hence, in order to obtain a 'clean' injection of a slug of reactant Y into a stream of X, *both* voltages V_{AD} and V_{BC} must be switched synchronously between the values required [and calculated using eqns. (9) and (10)] for the loading, injection and flow phases. This highlights the necessity for automated computer control of the applied voltages in micro-reactor devices.

It is, of course, possible to operate the micro-reactor such that the contents of reservoirs A and B are made to flow into the detection channel EH in different ratios controlled by the applied voltages (as opposed to the load, inject, flow sequence described above). Fig. 3 shows the ratio I_2/I_1 for different ratios of the applied voltages V_{AD}/V_{BC} at constant V_{BC}. Since the ratio of electrical currents is equal to the ratio of electroosmotic flow rates, the plot demonstrates that the mixing ratio of the flowing streams can be varied continuously by adjustment of the voltage ratio. (It should be noted that the current and voltage ratios in Fig. 3 are invariant with the absolute magnitudes of either current or voltages.) Fig. 3 also shows a similar plot in which the voltage V_{AD} is held constant. These calculations demonstrate that, in principle, the applied voltages can be used to vary

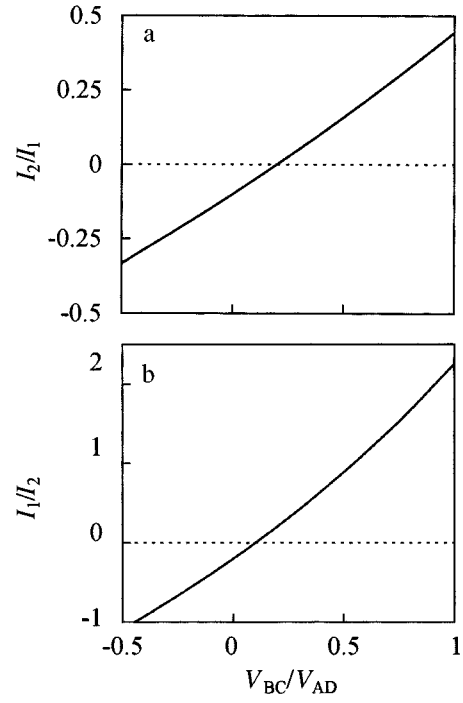

Fig. 3 Variation of I_2/I_1 with V_{AD}/V_{BC} (a) and I_1/I_2 with V_{BC}/V_{AD} (b). The calculations are for the micro-reactor configuration of Fig. 1 (assuming constant resistance per channel length) for channel lengths AE = CG = FB = HD = 10 mm, EF = FG = 5 mm and GH = 20 mm. The plots show the voltage ratios required (for this particular configuration) to obtain zero EOF in the injection circuit during loading/flow and zero EOF in the loading/flow circuit during injection.

continuously the ratio of concentrations of X and Y entering the detection channel. This type of micro-reactor manifold control can therefore be used, for example, to determine calibration data in analytical systems[53] or to investigate the concentration dependence of reaction kinetics under voltage control without refilling of the reservoirs.

It should be noted that this analysis, although revealing the basic principles, is somewhat simplistic in that hydrodynamic effects associated with the flows across manifold junctions and surface conductivity effects are neglected. More sophisticated modelling, as described, for example, in refs. 47, 48, 51 and 52, show that complex flow patterns around manifold junctions may significantly modify slug profiles obtained by the injection procedure. Additionally, non-zero surface conductivity would require modification of the equations presented here.

5 Control of chemical reactions under electroosmotic and electrophoretic flow

We take as the starting point a channel containing species X with a rectangular slug of reactant Y as would be obtained from a perfect load–inject–flow sequence (shown in Fig. 1). We assume here that species movement within the channel is controlled only by EOF and electrophoresis, *i.e.*, that pressure driven flow is absent. Under these conditions, the species' velocity profiles across the channel are flat (except for the region very close to the channel wall). Hence all concentrations vary only in the direction of the channel long axis x but are uniform in both orthogonal directions across the channel.

We consider a section of channel of length $2a$ centred at $x = 0$ and extending from $x = -a$ to $x = +a$. For the purpose of the numerical calculations, we adopt a moving coordinate system such that $x_{lab} = x + v_{os}t$, where x_{lab} is the x coordinate relative to the laboratory, v_{os} is the linear electroosmotic velocity and t is time. Initially the channel contains species X at concentration C_X^0 with a rectangular slug of species Y at concentration C_Y^0. The slug of Y has a width of $2b$ and is initially centred at $x = 0$. As described above, X and Y can react reversibly to form product Z with forward rate constant k_f (second order) and reverse rate constant k_r (first order). The initial conditions are stated as follows:

$$\begin{array}{lllll} -b \leqslant x \leqslant b: & C_X = 0, & C_Y = C_Y^0 & \text{at } t = 0 \\ \pm b \leqslant x \leqslant \pm a: & C_X = C_X^0, & C_Y = 0 & \text{at } t = 0 \\ -a \leqslant x \leqslant a: & C_Z = 0, & & \text{at } t = 0 \end{array} \quad (11)$$

Species X, Y and Z have diffusion coefficients D_X, D_Y and D_Z and move (relative to $x = 0$) with electrophoretic velocities v_{phX}, v_{phY} and v_{phZ}, respectively. We assume that all diffusion coefficients are invariant with concentration and that all thermal effects (arising, for example, from heats of reaction) are negligible. The concentrations of X, Y and Z are functions of both time and x according to the following set of equations:[68]

$$\begin{aligned} \frac{\partial C_X}{\partial t} &= D_X \frac{\partial^2 C_X}{\partial x^2} - k_f C_X C_Y + k_r C_Z - v_{phX} \frac{\partial C_X}{\partial x} \\ \frac{\partial C_Y}{\partial t} &= D_Y \frac{\partial^2 C_Y}{\partial x^2} - k_f C_X C_Y + k_r C_Z - v_{phY} \frac{\partial C_Y}{\partial x} \\ \frac{\partial C_Z}{\partial t} &= D_Z \frac{\partial^2 C_Z}{\partial x^2} + k_f C_X C_Y - k_r C_Z - v_{phZ} \frac{\partial C_Z}{\partial x} \end{aligned} \quad (12)$$

These equations correspond to the simple reaction scheme of eqn. (6) but more complex reaction schemes are easily incorporated. The situation described here for micro-reactors is identical (from a theoretical point of view) with that of electrophoretically mediated microanalysis (EMMA) described both experimentally and theoretically by Regnier *et al.*[69–72] Additionally, a related set of equations have been used recently to describe the elution characteristics of species undergoing a first-order reaction in a capillary electrophoresis system.[73]

The boundary conditions are taken to be that the concentrations of X, Y and Z are unperturbed from their initial values at $x = \pm a$, *i.e.*,

$$C_X(x = \pm a) = C_X^0, C_Y(x = \pm a) = C_Z(x = \pm a) = 0 \quad (13)$$

The use of these boundary conditions restricts the analysis to conditions such that the zone of reaction is far from the channel ends. For the manifold configuration shown in Fig. 1, this is valid since we wish to simulate the concentration changes occurring in the detection channel section GH before the reaction zone moves round the corner into section HD. The series of eqns. (11)–(13) is solved numerically to obtain plots of C_X, C_Y and C_Z *versus* x_{lab} for different times. The numerical algorithm, outlined in the Appendix, was implemented in a Visual Basic program running in EXCEL on a PC.

6 Example calculations

We first model the time evolution of the concentration profiles for a reaction in which all species X, Y and Z are uncharged. All other conditions are specified in the legend of Fig. 4. In this case, all reaction species move together in the channel with the electroosmotic velocity v_{os} and mixing of the reactants occurs only by inter-diffusion between the X stream and slug of Y. Fig. 4 shows three 'snapshots' of the concentration profiles where it can be seen that product Z is formed only at the trailing and leading edges of the slug of Y where diffusional inter-mixing gives finite concentrations of both X and Y. Because the time

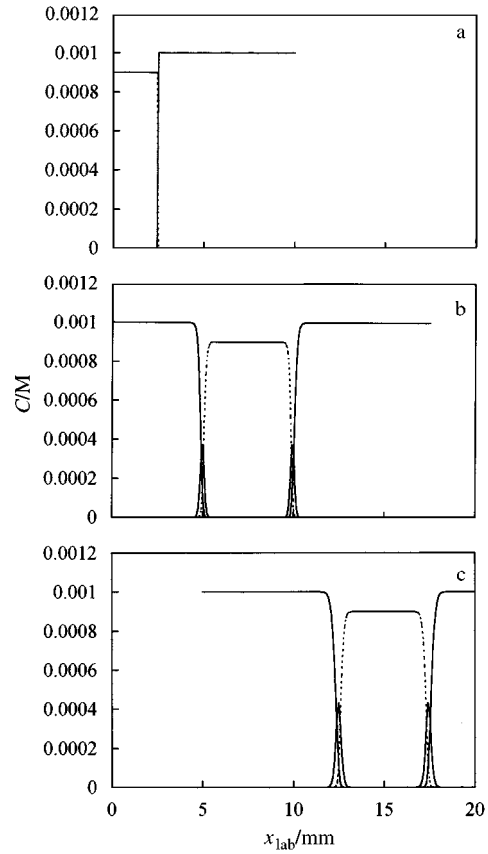

Fig. 4 Calculated concentration profiles for C_X (solid line), C_Y (dashed line) and product C_Z (solid line) for time = 0 (a), 15 (b) and 30 s (c). The parameters are $C_X^0 = 1$ mM, $C_Y^0 = 0.9$ mM, $C_Z^0 = 0$ mM, $D_X = 1 \times 10^{-9}$ m^2 s^{-1}, $D_Y = 0.7 \times 10^{-9}$ m^2 s^{-1}, $D_Z = 0.5 \times 10^{-9}$ m^2 s^{-1}, $v_{os} = 0.5$ mm s^{-1}, $k_f = 1000$ l mol^{-1} s^{-1}, $k_r = 0$ s^{-1}, slug width ($2b$) = 5 mm and all electrophoretic velocities set equal to zero (*i.e.*, all species are uncharged).

required for reactant diffusion across the width of the slug of Y is long relative to the time the slug takes to traverse the detection channel EH, the extent of product formation is low.

The behaviour of charged reactant species is very different. We simulate the case in which X and Z both bear a positive charge and Y is uncharged. Within the electric field, the velocities of X and Z are accelerated relative to v_{os} whereas Y moves with velocity v_{os}. As seen in Fig. 5, the difference in electrophoretic velocities of the different species causes a displacement of the slug of Y relative to the 'gap' in the concentration profile of X. This gives a greatly increased mixing of X and Y (with concomitant formation of Z) at the trailing edge of the Y slug. The extent of product formation within the detection time is therefore greatly increased relative to that for the case of uncharged reagents. Changing the signs of the charges on both X and Z from positive to negative (calculations not shown) causes the product formation to occur at the leading (rather than the trailing) edge of the slug. We note here that it is not necessary for the species X and Y to have different sign charges to induce displacement of the slug of Y relative to the 'gap' in X. Even with the same (non-zero) charges, X and Y will have different electrophoretic velocities, and thus show displacement, so long as their diffusion coefficients are different [see eqn. (5)].

For the case in which X and Z bear charges, and Y is neutral as in Fig. 5, the extent of product formation is largely controlled by the relative rate of displacement of the concentration profiles of X and Y. In turn, this is determined by their relative electrophoretic velocities which, like v_{os}, scale with the applied electric field. Fig. 6 shows the effect of increasing the electric field which is modelled by increasing v_{os} whilst maintaining v_{ph} for the different species at constant ratios relative to v_{os}. The ordinate of Fig. 6 shows the integral of the product concentration profile, integrated over the detection channel length. (For an optically absorbing species Z with the absorbance detection configuration of Fig. 1, the measured absorbance signal is proportional to this integral.) It can be seen that the applied voltage can be used to control the extent of product formation. The minimum value of product formation is obtained with zero voltage when the extent of product formation is determined only by inter-diffusion of X and Y without the aid of electrophoretic displacement of the concentration profiles. Sufficiently high applied voltage produces virtually complete displacement and complete conversion of Y to product.

As seen above, the time required for complete reaction of the Y slug is determined largely by the time taken for the slug to be displaced from the 'gap' in the concentration profile of X and should therefore decrease as the slug width is decreased. Simulation of this effect is shown in Fig. 7, where it can be seen that 100% product conversion can be achieved (at a particular applied voltage) by reducing the width sufficiently. Obviously, in the simulation shown, the total amount of product formed reduces as the initial width of the Y slug is decreased. However, it would of course be possible to inject multiple slugs of Y, so as to increase the total amount of product formation simultaneously with increasing the percentage conversion. We note here that techniques to produce very narrow slugs (μm) have been demonstrated experimentally.[74] At sufficiently small widths, diffusion alone would ensure complete reactant mixing and conversion of the Y slug to product.

We next examine the effects of varying the forward rate constant of the chemical reaction. As seen above, for the concentrations used in the simulation with k_f = 1000 l mol^{-1} s^{-1}, the extent of chemical reaction is largely controlled by the time required for inter-mixing of the reagents. Under

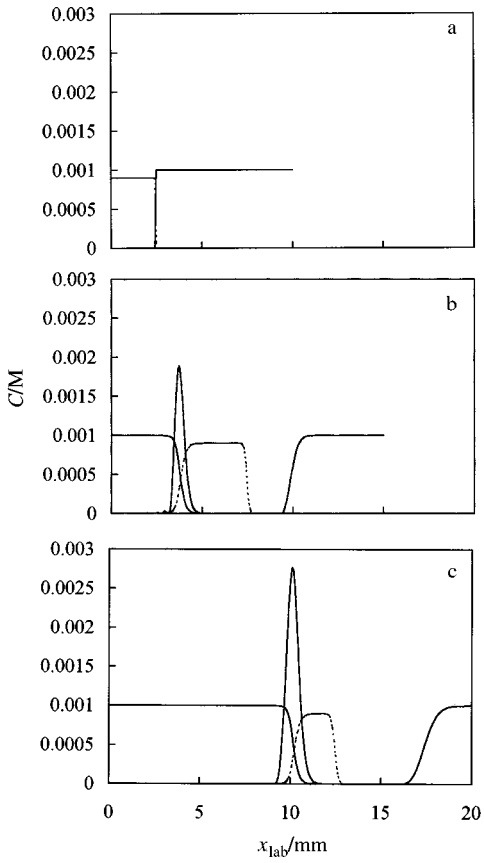

Fig. 5 Calculated concentration profiles for the conditions of Fig. 4 except that v_{phX} = 0.5, v_{phY} = 0 and v_{phZ} = 0.25 mm s^{-1}. This corresponds to the species X and Z both bearing a positive charge (which serve to accelerate their total motion) and Y being uncharged.

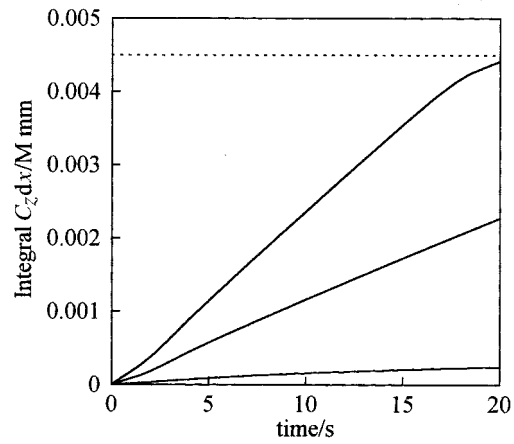

Fig. 6 Variation of the integral of the product concentration profile with time for different v_{os} equal to 0, 0.5 and 1 mm s^{-1} for the curves in ascending order. The electrophoretic velocities were held at v_{phX} = v_{os}, v_{phY} = 0 and v_{phZ} = v_{os}/2 with other conditions as for Fig. 5. The horizontal dashed line corresponds to total conversion to product.

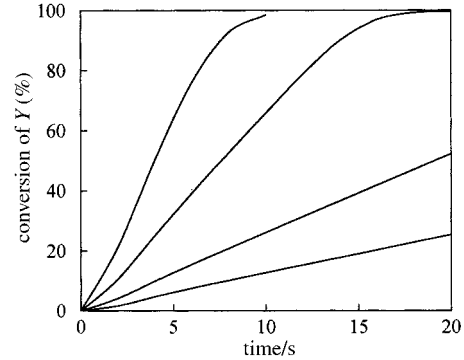

Fig. 7 Variation of percentage conversion of Y with time for (in ascending order) initial width of the slug of Y equal to 10, 5, 2 and 1 mm. All other conditions were as for Fig. 5.

these conditions, increasing k_f gives virtually no change in the extent of product formation (Fig. 8) since chemical reaction is already faster than the inter-mixing of X and Y. Reducing k_f to lower values causes product formation to decrease as the rate-determining step switches from mixing to the chemical reaction step. Concentration profiles for reactions where product formation is controlled either by mixing or by chemical reaction are compared in Fig. 9. We note here that the transition from mixing rate control to chemical reaction rate control may be induced either by changing the forward rate constant or by changing the reactant concentrations since forward reaction rate is equal to the product $k_f C_X C_Y$.

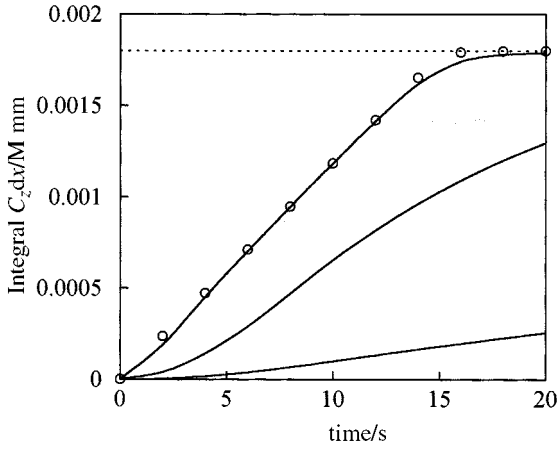

Fig. 8 Variation of integral C_Zdx with time for (in ascending order) k_f = 10, 100 and 1000 l mol^{-1} s^{-1}. The initial width of the slug of Y was 2 mm and all other conditions were as for Fig. 5. The open circles were calculated for k_f = 10 000 l mol^{-1} s^{-1} and correspond to the fast reaction limit under these conditions. The horizontal dashed line corresponds to total conversion to product.

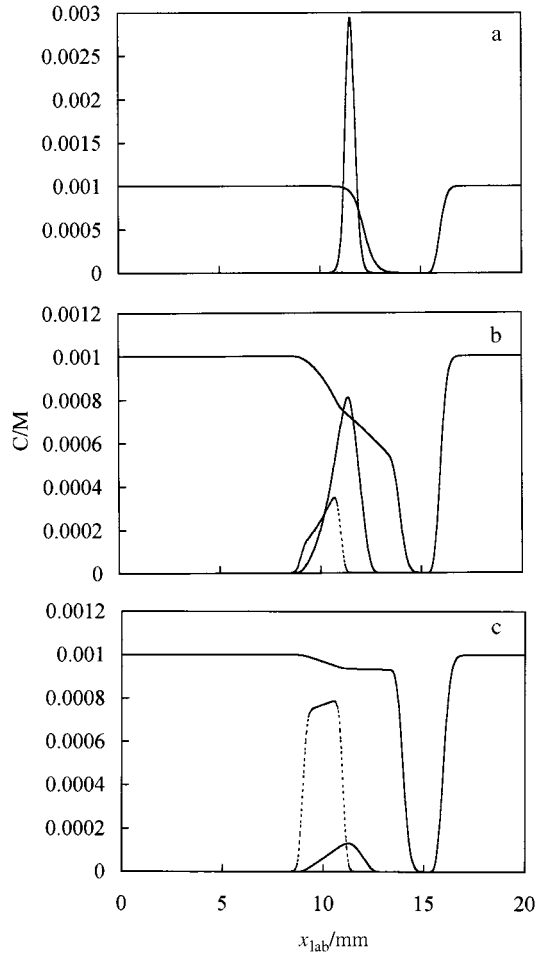

Fig. 9 Concentration profiles of X, Y (dashed line) and Z after 20 s for k_f = 1000 (a), 100 (b) and 10 l mol^{-1} s^{-1} (c). All other conditions were as for Fig. 8.

The simulations highlight the importance of a number of time-scales in considering second-order chemical reactions in micro-reactor manifolds. Definitions of the time-scales appropriate to the manifold configuration discussed here are as follows:

$$t_{diffusion} = b^2/D \quad (14)$$

$$t_{chemical} = 1/k_f C_X^0 \quad (15)$$

$$t_{displacement} = 2b/|v_{phX} - v_{phY}| \quad (16)$$

$$t_{detection} = l_{detection}/(v_{os} + v_{phY}) \quad (17)$$

where $t_{diffusion}$ is the time required for inter-diffusional mixing of X and Y across the slug of Y (width 2b) to occur. In this context, D is the mean of D_X and D_Y. $t_{chemical}$ is the time required for chemical reaction between X and Y (under conditions when $C_X^0 > C_Y^0$). $t_{displacement}$ is the time required to displace completely the slug of Y from the 'gap' in the concentration profile of X. $t_{detection}$ is the time spent by the slug of Y within the detection channel of length $l_{detection}$. Consideration of the relative magnitudes of these times allows a crude prediction of the behaviour of a chemical reaction within a microreactor system. Virtually complete conversion to product is expected when $t_{detection} > t_{displacement}$ (or $t_{diffusion}$) and $t_{chemical}$. The extent of product formation is controlled by the applied voltage (by control of v_{ph}) when $t_{detection} < t_{displacement}$ and $t_{displacement} > t_{chemical}$. Under these conditions, the product formation is insensitive to the chemical reaction rate and the initial concentration of X but is controlled by the applied voltage. When $t_{detection} < t_{chemical}$ and $t_{chemical} > t_{displacement}$ or $t_{diffusion}$, product formation is sensitive to the chemical rate constant, the reactant concentrations and the applied voltage. These considerations apply to the simple load–inject–flow voltage control sequence described earlier. However, as demonstrated elegantly by Regnier's group in the context of EMMA, more complex voltage control sequences can be used to control the extent of reaction.[69–72]

Finally, we consider the effect of introducing reversibility into the chemical reaction. Under conditions when the reaction reaches its final, equilibrium extent of product formation before exiting the detection channel section, the final value reached decreases with increasing k_r as shown in Fig. 10. In this situation, when displacement and chemical reaction are complete, the final extent of product formation is primarily controlled by the equilibrium constant K (= k_f/k_r) and C_X^0.

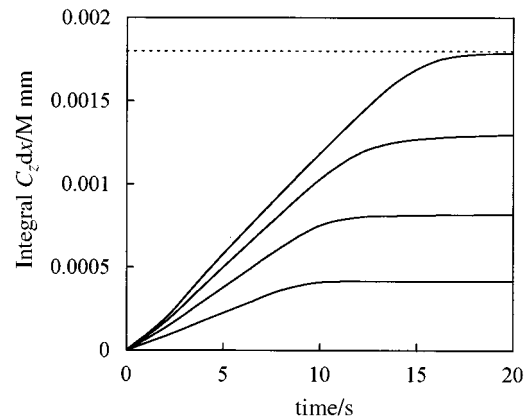

Fig. 10 Variation of integral C_Zdx with time for k_f = 1000 l mol^{-1} s^{-1} and (in ascending order) k_r = 3, 1, 0.3 and 0 s^{-1}. All other conditions were as for Fig. 8. The horizontal dashed line corresponds to total conversion to product.

The simulations illustrate that product formation in micro-reactor manifolds may (under different conditions) be sensitive to the applied voltage, the chemical rate constants, concentrations, diffusion constants and species charge. In principle, micro-reactor investigation of reactions can yield information on all these physico-chemical properties. For the simulations, the range of input parameters were chosen to be realistic for the type of reaction that may be studied. For example, in aqueous solution at pH 7 and 25 °C, the complex formation reaction Ni^{2+} + PADA gives $NiPADA^{2+}$ has k_f = 1300 l $mol^{-1}s^{-1}$ and k_r = 0.1 s^{-1} where PADA is pyridine-2-azo-*p*-dimethylaniline.[75,76] Ni^{2+} and the NiPADA complex both have a charge of +2 whereas PADA is uncharged. The value of D for Ni^{2+} is 1.25×10^{-9} m^2 s^{-1}.[77] Since PADA has a larger molecular volume than Ni^{2+}, it is expected to have a lower diffusion coefficient (approximately half). Similarly, the complex is expected to have a D value lower than that of either reactant. Hence the physico-chemical properties of the Ni–PADA reaction are such that the simulation parameters should correspond approximately to somewhere between those of the top two curves of Fig. 10. For the Ni–PADA reaction, the molar absorptivity of the complex product is approximately 32 000 l mol^{-1} cm^{-1} at the wavelength corresponding to maximum absorption.[75] Using the spectrophotometric detection configuration described here, the integrated product concentration profile would produce a large absorbance signal, easily detectable with good precision.

7 Conclusions and future outlook

The theoretical principles and calculations described in this tutorial review provide the basis for understanding the behaviour of chemical reactions within micro-reactor manifolds with electrokinetic flow control. The aim has been to provide principles to guide the design and development of such systems and the main conclusions are as follows:

1. EOF is determined primarily by the zeta potential of the channel/solution interface and gives a uniform velocity profile across the channel except very close (nm) to the channel wall. Non-uniform velocity profiles may be caused by pressure gradients arising from unequal reservoir heights, Laplace pressure effects resulting from the liquid menisci within the reservoirs and non-uniformity of the cross-sectional areas and zeta potential of the channels. Non-uniform zeta potentials may arise owing to specific adsorption of reagents in different channel sections or when the different channel sections are constructed of different materials. These complicating factors require careful experimental control in order to obtain accurate, reproducible results in micro-reactor systems.

2. Analysis of the dc circuit equivalent to the micro-reactor configuration allows the proper calculation of the voltages required for a 'clean' injection of a reactant slug into a stream of a second reactant.

3. The temporal and spatial evolution of a chemical reaction under EOF and electrophoretic control is determined primarily by the relative magnitudes of $t_{diffusion}$, $t_{chemical}$, $t_{displacement}$ and $t_{detection}$. Proper adjustment of the relative magnitudes of these different time-scales allows the extent of product conversion to be controlled by the voltages applied to the micro-reactor device.

The potential power of micro-reactor manifolds lies in the fact that complex channel labyrinths can be accommodated within a small device and that they allow the investigation of chemical reactions to be made under computer control. From the results described here, measurement of the extent of product conversion under different voltage conditions should, in principle, yield quantitative information on reaction rate parameters and charge/diffusion properties of the reactant species. It is technically feasible to construct micro-reactor manifolds in which many reactions could be investigated either in sequence or simultaneously using automated computer control. Such a development would go some way towards realising the 'Lab-on-a-Chip' concept and would provide a quantum leap in the rate of accumulation of physico-chemical information for analytical, general chemical, biochemical and catalytic reactions. Analogously to a conventional electronic chip, the main function of such a device would be rapid gathering and processing of chemical information.

In this paper, we have discussed a simple homogeneous liquid phase reaction, but many other possibilities can be envisaged. The areas of homogeneous and heterogeneous catalysis, in particular, could benefit from the high speed, high throughput experimentation possibilities of micro-reactors. In this connection, it has recently been demonstrated that glass frits may be incorporated within a micro-reactor channel.[78] Further, a palladium catalyst supported on such a frit has been used successfully to catalyse reactions within a manifold under EOF control.[79] It was demonstrated that the spatial and temporal control of reactants could be used to deliver a first reagent to a catalyst surface followed by a second reagent after a controllable time period. This type of detailed control is generally impossible (at least within the short time-scales achievable in micro-reactors) in the usual situation of stirring a reagent mixture over a slurry of catalyst. In analytical terms, such an approach could mean controlling the output from a chemiluminescent reaction accurately at a specific detector site.[80] Some of these possibilities are currently being pursued further in the authors' laboratories.

8 Appendix

8.1 Numerical algorithm for the solution of eqns. (11)–(13)

We use the fact that the diffusion–reaction eqns. (12) have virtually similar form:

$$\frac{\partial C_k}{\partial t} + v_{ph_k}\frac{\partial C_k}{\partial x} = D_k\frac{\partial^2 C_k}{\partial x^2} + S_k(x,t) \qquad (k = X, Y, Z) \qquad \text{(A1)}$$

where $S_k(x,t)$ are the source terms which depend on x and t through the rates of the respective chemical reactions. In our particular case of chemical reaction, eqn. (6), we have

$$S_X = S_Y = -S_Z = k_r C_Z(x,t) - k_f C_X(x,t) C_Y(x,t) \qquad \text{(A2)}$$

To find the evolution of the concentration profiles, $C_k(x,t)$, with time we use a semi-implicit Crank–Nicholson method for integration of eqns. (A1).[81,82] For the convenience of readers we give here the details of the numerical scheme applied to eqns. (A1). To avoid overburden, we omit the subscript k in our further notations. The space and time are discretised as follows:

$$x_i = (i-1)\Delta x, \quad t_j = (j-1)\Delta t, \quad i = 1, 2, \ldots, n; \quad j = 1, 2, \ldots \qquad \text{(A3)}$$

where Δx and Δt are the spatial and time steps. Since eqns. (A1) are highly non-linear owing to the source terms, an appropriate linearisation is needed. In our calculations we apply the Crank–Nicholson scheme as follows:

$$\left(\frac{\partial C}{\partial t}\right)_i = \frac{1}{2}\left\{D\left[\left(\frac{\partial^2 C}{\partial x^2}\right)_{i,j+1} + \left(\frac{\partial^2 C}{\partial x^2}\right)_{i,j}\right] - v_{ph}\left[\left(\frac{\partial C}{\partial x}\right)_{i,j+1} + \left(\frac{\partial C}{\partial x}\right)_{i,j}\right]\right\} + [S(x,t)]_{i,j} \qquad \text{(A4)}$$

where the non-linear terms, S, are estimated by using only information from the previous time step (j) or from the initial

conditions ($j = 0$). We remark that the coupling between the three eqns. (A1) comes from the source terms. That is why the resulting equations after the above discretisation are semi-decoupled in the framework of a single time step. Thus, the substitution of the partial derivatives in eqn. (A4) by finite difference approximations

$$\left(\frac{\partial C}{\partial t}\right)_i = \frac{C_{i,j+1} - C_{i,j}}{\Delta t} + O(\Delta t)$$
$$\left(\frac{\partial C}{\partial t}\right)_i = \frac{C_{i+1,j} - C_{i-1,j}}{2\Delta x} + O(\Delta x^2) \quad \text{(A5)}$$
$$\left(\frac{\partial^2 C}{\partial x^2}\right)_i = \frac{C_{i+1,j} - 2C_{i,j} + C_{i-1,j}}{\Delta x^2} + O(\Delta x^2)$$

gives a system of linear equations describing each of the profiles in the next time ($j + 1$) step:

$$\beta(1 + a)C_{i+1,j+1} - (1 + 2\beta)C_{i,j+1} + \beta(1 - \alpha)C_{i-1,j+1} = \gamma_i, \quad i = 2, \ldots, n - 1 \quad \text{(A6)}$$

where

$$\alpha = \frac{v\Delta x}{2D}, \beta = \frac{D\Delta t}{2\Delta x^2}, \quad \text{(A7)}$$
$$\gamma_i = S_{i,j}\Delta t - \beta(1+\alpha)C_{i-1,j} - (1-2\beta)C_{i,j} - \beta(1-\alpha)C_{i+1,j}$$

The implication of the boundary conditions, eqns. (11), requires that

$$C_{i,j+1} = C_{n,j+1} = C_0 \quad \text{(A8)}$$

where $C_0 = C_X^0$ for X profile and $C_0 = 0$ for Y and Z profiles. Initially, stepwise profiles are used as an initial condition, according to eqns. (11). We solve the three-diagonal system of linear eqns. (A6) by using the Thomas algorithm[81] to obtain the new concentration profiles ($j + 1$), which then are used to calculate γ_i for the next time step, *etc*. Once the spatial step-size Δx has been selected, the time step Δt is controlled to maintain the stability of the numerical method. We should stress that the accuracy of this numerical scheme decreases when the chemical reaction is much faster than the respective diffusion process ($t_{diffusion} >> t_{chemical}$). In this case we recommend the use of the fully implicit Crank–Nicholson scheme.[81]

8.2 Symbols

A–D	reservoirs
a	half-length of channel
$A_{channel}$	cross-sectional area of channel
b	initial half-width of rectangular slug of reactant Y
C_X	concentration of species X
C_X^0	initial concentration of species X
D_X	diffusion coefficient of species X
E–H	channel corners
E	electric field
e	electronic charge
g	acceleration due to gravity
i, j	indices for space and time steps used in the numerical calculations
I_1	electrical current in loop 1
k	Boltzmann constant
K	equilibrium constant for reaction
k_f	second-order forward rate constant
k_r	first-order reverse rate constant
$l_{channel}$	channel length
$l_{detection}$	length of detection channel section
r	radius of curvature of liquid meniscus in reservoir
R_{AE}	resistance across channel section AE
$R_{loop\ 1}$	sum of resistances across channel sections comprising loop 1
$S(x,t)$	source terms
T	absolute temperature
t	time
$t_{chemical}$	time required for chemical reaction
$t_{detection}$	time required for Y slug to traverse the detection channel section
$t_{diffusion}$	time required for diffusion across the rectangular slug of Y
$t_{displacement}$	time required for displacement of slug of Y from 'gap' in X concentration profile
V_{AD}	applied voltage across reservoirs A and D
V_{os}	EOF driven volumetric flow rate
v_{os}	linear electroosmotic flow velocity
v_{phX}	electrophoretic velocity of species X
V_{press}	pressure driven flow rate
x	co-ordinate along channel normalised with respect to v_{os}
X, Y, Z	reactant species
x_{lab}	coordinate along channel in laboratory coordinates
z	number of electronic charges on an ionic species
Δh_{res}	height difference between reservoirs
ΔP	hydrostatic pressure difference between reservoirs
ε	relative permittivity
ε_0	permittivity of free space
γ	liquid/air surface tension
η	viscosity of liquid in the channel
λ_0	electrical conductivity of liquid
ρ	liquid density
ζ	zeta potential of the channel/liquid interface

9 References

1 A. Manz, D. J. Harrison, E. Verpoorte, J. C. Fettinger, H. Lüdi and H. M. Widmer, *Chimia*, 1991, **45**, 103.
2 A. Manz, D. J. Harrison, E. Verpoorte and H. M. Widmer, *Adv. Chromatogr*., 1993, **33**, 1.
3 A. Manz, C. S. Effenhauser, N. Barggraf, E. J. M. Verpoorte, D. E. Raymond and H. M. Widmer, *Analusis*, 1994, **22**, M25.
4 A. T. Woolley, and R. A. Mathies, *Anal. Chem*., 1995, **67**, 3676.
5 A. T. Woolley, D. Hadley, P. Ladre, A. J. deMello, R. A. Mathies and M. A. Northrup, *Anal. Chem.*, 1996, **78**, 4843.
6 A. T. Woolley, G. F. Sensabaugh and R. A. Mathies, *Anal. Chem.*, 1997, **69**, 2181.
7 A. T. Woolley and R. A. Mathies, *Proc. Natl. Acad. Sci. USA*, 1994, **91**, 11348.
8 S. C. Jacobson and J. M. Ramsey, *Anal. Chem*., 1996, **68**, 720.
9 P. C. Simpson, D. Roach, A. T. Woolley, T. Thorsen, G. F. Sensabaugh and R. A. Mathies, *Proc. Natl. Acad. Sci. USA*, 1998, **95**, 2256.
10 R. F. Service, *Science*, 1998, **282**, 399.
11 A. Manz, E. J. M. Verpoorte, C. S. Effenhauser, N. Barggraf, D. E. Raymond and H. M. Widmer, *Fresenius' J. Anal. Chem*., 1994, **348**, 567.
12 H. Y. Wang, R. S. Foote, S. C. Jacobson, J. H. Schneibel and J. M. Ramsey, *Sens. Actuators B*, 1997, **45**, 199.
13 Z. H. Fan and D. J. Harrison, *Anal. Chem*., 1994, **66**, 177.
14 D. J. Harrison, K. Fluri, N. Chiem, T. Tang and Z. Fang, *Sens. Actuators B*, 1996, **33**, 105.
15 D. J. Harrison, P. G. Glavina and A. Manz,, *Sens. Actuators B*, 1993, **10**, 107.
16 M. A. Roberts, J. S. Rossier, P. Bercier and H. Girault, *Anal.Chem.*, 1997, **69**, 2035.
17 L. E. Locasico, *Anal. Chem.*, 1997, **69**, 4783.
18 W. Ehrfeld and H. Lehr, *Radiat. Phys. Chem.*, 1995, **45**, 349.
19 D. C. Duffy, J. Cooper McDonald, O. J. A. Schueller and G. M. Whitesides, *Anal. Chem.*, 1998, **70**, 4974.
20 H.-J. Ache, in *Micro Total Analytical Systems*, ed. A. van den Berg and P. Bergveld, Kluwer, Dordrecht, 1995, p. 47.

21 R. Vökel, H. P. Herzig, P. Nussbaum and R. Dändliker, *Opt. Eng.*, 1996, **35**, 3323.
22 E. Verpoorte, A. Manz, H. Lüdi, A. E. Bruno, F. Maystre, B. Krattiger, H. M. Widmer, B. H van der Schoot and N. F. de Rooij, *Sens. Actuators B*, 1992, **6**, 66.
23 D. J. Harrison, K. Fluri, K. Seiler, Z. Fan, C. S. Effenhauser and A. Manz, *Science*, 1993, **261**, 895.
24 S. C. Jacobson and J. N. Ramsey, *Anal. Chem*., 1996, **68**, 720.
25 C. S. Effenhauser, G. J. M. Bruin, A. Paulus and M. Ehrat, *Anal. Chem*., 1978, **69**, 3451.
26 A. T. Woolley and R. A. Mathies, *Anal. Chem*., 1995, **67**, 3676.
27 D. J. Harrison, A. Manz, Z. Fan, H. Lüdi and H. M. Widmer, *Anal. Chem*., 1992, **64**, 1926.
28 N. Chiem and D. J. Harrison, *Anal. Chem*., 1997, **69**, 373.
29 D. E. Raymond, A. Manz and H. M. Widmer, *Anal. Chem*., 1996, **66**, 2858.
30 C. S. Effenhauser, A. Manz and H. M. Widmer, *Anal. Chem*., 1995, **67**, 2284.
31 S. C. Jacobson and J. M. Ramsey, *Anal. Chem*., 1997, **67**, 3212.
32 S. C. Jacobson, R. Hergenröder, L. B. Koutny and J. M. Ramsey, *Anal. Chem*., 1994, **66**, 1114.
33 S. C. Jacobson, L. B. Koutny, R. Hergenröder, A. W. Moore and J. M. Ramsey, *Anal. Chem*., 1994, **66**, 3472.
34 L. C. Waters, S. C. Jacobson, N. Kroutchinina, J. Khandurina, R. S. Foote and J. M. Ramsey, *Anal. Chem*., 1998, **70**, 5172.
35 M. U. Kopp, A. J. deMello and A. Manz, *Science*, 1998, **280**, 1046.
36 C. S. Effenhausaer and A. Manz, *Am. Lab.*, 1994, **26**, 15.
37 G. Blankenstein and U. D. Larsen, *Biosens. Bioelectron.*, 1998, **13**, 427.
38 S. Sundberg, A. Copfsill, R. Nagle, S. Gallagher, C. Chow, G. Wada, T. Nikiforov and J. W. Parce, *Am. Lab*., 1998, **30**, 22.
39 R. Kniss, *Am. Lab*., 1998, **30**, 40.
40 P. Graveson, J. Branebjerg and O. S. Jensen, *J. Micromech. Microeng*., 1993, **3**, 168.
41 S. Shoji and M. Esashi, *J. Micromech. Microeng*., 1994, **4**, 157.
42 P. K. Dasgupta and S. Liu, *Anal. Chem*., 1994, **66**, 1792.
43 R. Zengerle, J. Ulrich, S. Kluge, M. Richter and A. Richter, *Sens. Actuators A*, 1995, **50**, 81.
44 A. Manz, C. S. Effenhauser, N. Burggraf, D. J. Harrison, K. Seiler and K. Fluri, *J. Micromech. Microeng*., 1994, **4**, 257.
45 P. H. Paul, D. W. Arnold and D. J. Rakestraw, in *Micro Total Analysis Systems '98*, ed. D. J. Harrison and A. van den Berg, Kluwer, Dordrecht, 1998, p. 49.
46 G. Boer, A. Dodge, K. Fluri, B. H. van der Schoot, E. Verpoorte and N. F. de Rooij, in *Micro Total Analysis Systems '98*, ed. D. J. Harrison and A. van den Berg, Kluwer, Dordrecht, 1998, p. 53.
47 S. C. Jacobson, R. Hergenröder, L. B. Koutny, R. J. Warmack and J. M. Ramsey, *Anal. Chem*., 1994, **66**, 1107.
48 S. C. Jacobson, R. Hergenröder, A. W. Moore and J. M. Ramsey, *Anal. Chem*., 1994, **66**, 4127.
49 K. Seiler, Z. H. Fang, K. Fluri and D. J. Harrison, *Anal. Chem*., 1994, **13**, 3485.
50 P. H. Paul, M. G. Garguilo and D. J. Rakeshaw, *Anal. Chem*., 1998, **70**, 2459.
51 S. V. Ermakov, S. C. Jacobson and J. M. Ramsey, in *Micro Total Analysis Systems '98*, ed. D. J. Harrison and A. van den Berg, Kluwer, Dordrecht, 1998, p. 149.
52 N. A. Patankar and H. H. Hu, *Anal. Chem*., 1998, **70**, 1870.
53 S. J. Haswell, *Analyst*, 1997, **122**, 1R.
54 L J. Kricka and P. Wilding, in *Handbook of Clinical Automation, Robotics and Optimisation*, ed. G. J. Kost and J. Welsh, John Wiley & Sons, New York, 1996, p. 45.
55 G. T. A. Kovacs, *Micromachined Transducers Sourcebook*, WCB/ McGraw-Hill, Boston, .
56 G. T. A. Kovacs, K. Petersen and M. Albin, *Anal. Chem*., 1996, **68**, 407A.
57 G. N. Doku and S. J. Haswell, *Anal. Chim. Acta*, 1999, **382**, 1.
58 G. M. Greenway, S. J. Haswell and P. Petsul, *Anal. Chim. Acta*, 1999, **387**, 1.
59 C. L. Rice and R. Whitehead, *J. Phys. Chem*., 1965, **69**, 4017.
60 R. J. Hunter, *Zeta Potential in Colloid Science*, Academic Press, London, 1981.
61 J. Jednacak, V. Pravdic and W. Haller, *J. Colloid Interface Sci*., 1974, **49**, 16.
62 G. R. Wiese, R. O. James and T. W. Healy, *Discuss. Faraday Soc*., 1971, **52**, 302.
63 A. Vernhet, M. N. Bellon-Fontaine and A. Doren, *J. Chim. Phys*., 1994, **91**, 1728.
64 R. A. Van Wagenen and J. D. Andrada, *J. Colloid Interface Sci*., 1979, **76**, 305.
65 M. P. Sidorova, I. A. Savina and L. E. Ermakova, *Colloid J*., 1996, **53**, 380.
66 See, for example, A. W. Adamson and A. P. Gast, *Physical Chemistry of Surfaces*, John Wiley and Sons, New York, 5th edn., 1997, p. 10.
67 See, for example, P. W. Atkins, *Physical Chemistry*, Oxford University Press, Oxford, 5th edn., 1994, p. 840.
68 See, for example, W. Jost, *Diffusion in Solids, Liquids and Gases*, Academic Press, New York, 1952.
69 B. J. Harmon, D. H. Patterson and F. E. Regnier, *Anal. Chem.*, 1993, **65**, 2655.
70 B. J. Harmon, I. Leesong and F. E. Regnier, *Anal. Chem*., 1994, **66**, 3797.
71 F. E. Regnier, D. H. Patterson and B. J. Harmon, *Trends Anal. Chem*., 1995, **14**, 177.
72 D. H. Patterson, B. J. Harmon and F. E. Regnier, *J. Chromatogr., A*, 1996, **732**, 119.
73 S. N. Semenov, *Anal. Commun.*, 1998, **35**, 411.
74 J. B. Knight, A. Vishwanath, J. P. Brody and R. H. Austin, *Phys. Rev. Lett*., 1998, **80**, 3863.
75 M. A. Cobb and D. N. Hague, *J. Chem. Soc., Faraday Trans. 1*, 1972, **68**, 932.
76 A. D. James and B. H. Robinson, *J. Chem. Soc., Faraday, Trans. 1*, 1978, **74**, 10.
77 V. N. M. Lobo and J. L. Quaresma, *Handbook of Electrolyte Solutions, Part B*, Elsevier, Amsterdam, 1989.
78 P. D. Christensen, S. W. P. Johnson, T. McCreedy, V. Skelton and N. G. Wilson, *Anal. Commun*., 1998, **35**, 341.
79 V. Skelton, S. J. Haswell, G. M. Greenway, P. Styring and D. O. Morgan, *Chem. Eur. J*., submitted for publication.
80 G. M. Greenway, L. Nelstrop and S. N. Port, *Anal. Chim. Acta*, in press.
81 See, for example, W. H. Press, S. A. Teukolsky, W. T. Vetterling and B. P. Flannery, *Numerical Recipes in FORTRAN*, Cambridge University Press, Cambridge, 2nd edn., 1992.
82 V. N. Paunov, K. D. Danov, N. Alleborn, H. Raszcilier and F. Durst, *Chem. Eng. Sci.*, 1998, **53**, 2839.

Paper 9/03624E